Particle tracking velocimetry and particle image velocimetry study of the slow motion of rough and smooth solid spheres in a yield-stress fluid

Yulia Holenberg,[1] Olga M. Lavrenteva,[1] Uri Shavit,[2] and Avinoam Nir[1]
[1]*Department of Chemical Engineering, Technion-Israel Institute of Technology, Haifa, 32000, Israel*
[2]*Department of Civil and Environmental Engineering, Technion-Israel Institute of Technology, Haifa, 32000, Israel*
(Received 28 August 2012; published 4 December 2012)

We report experimental evidence of an effect opposite to the "solidification" of small bubbles in liquid where the surface can become immobile. Namely, it is demonstrated that smooth solid spheres falling in a yield-stress fluid under the action of gravity can behave similar to drops. Particle tracking velocimetry was used to determine the shape of the yielded region around solid spherical particles undergoing slow stationary motion in 0.07% w/w Carbopol gel due to gravity under creeping flow conditions. The flow field inside the yielded region was determined by particle image velocimetry. It was found that the shape of the yielded region and the flow field around slow-moving rough particles is similar to the published results of numerical simulations, whereas those around smooth spheres resemble the experimental results obtained for viscous drops. The effect was explained by a slip of the gel on the smooth surface. Most likely, the slip originated from seepage of clean water from the gel, forming a thin lubricating layer near the solid surface.

DOI: 10.1103/PhysRevE.86.066301 PACS number(s): 47.50.−d, 47.80.Jk

I. INTRODUCTION

Motion of large particles in yield-stress fluids is important in many industrial applications such as, e.g., the lifting of excavated material in the oil industry, the movement of food suspensions, and the mixture of additives in the cosmetic and drug industries. Thus, numerous experimental, numerical, and analytical investigations were devoted to this subject.

When a particle moves in an otherwise quiescent yield-stress material, under the action of gravity or another external force, a region of flowing fluid (yielded region) appears near the body surface, while total stagnation may exist elsewhere. The determination of this yielded region as well as the flow pattern in it, are the important aspects of the relative motion of the inclusion inside the viscoplastic material.

Most of the studies available in the literature, so far, deal with the motion of a spherical solid particle in a viscoplastic matrix. Beris *et al.* [1] and Lui *et al.* [2] employed a finite elements method to calculate the size and shape of the yielded region around a spherical particle held in a steady creeping flow of an unbounded Bingham plastic. There are additional simulations of similar flows as well as of the motion of spheres in tubes filled with Bingham plastic [3] and Herschel-Bulkley material [4], which employed various regularization methods [2] to overcome the singular rheological expressions. De Besses *et al.* [5] simulated stationary motion around a sphere in Herschel-Bulkley fluid by considering slip boundary condition at the interface using the commercial software Fluent. The results of simulations confirm that at a very low velocity of the motion, when inertia is negligible, the flow has a symmetry with respect to a plane perpendicular to the flow and passing through the center of the sphere. However, the shapes of the yielded region obtained in different studies differ considerably. Most numerical simulations report on apparent unyielded islands inside the yielded regions attached to the polar caps and/or along the equatorial plane of the sphere. The study of Liu *et al.* [2] revealed that these inner apparent unyielded islands shrink with increasing regularization parameter, but their limiting behavior is unclear so far.

Results on experimental determination of the yielded region size and shape around a spherical solid particle reported in the literature [6–8] were obtained via various flow visualization methods. Atapattu *et al.* [6] employed a laser-speckle tracer method, while Putz *et al.* [7] and Gueslin *et al.* [8] used particle image velocimetry (PIV). Both optical flow visualization techniques allow tracking of the motion of small tracer particles, dispersed in the fluid before the experiment. The methods differ in tracer particles' concentration. The concentration of the seeded particles, acceptable for PIV, is such that individual particles at each image can be identified, but their motion cannot be tracked. In the images obtained by the laser-speckle method, individual particles cannot be identified due to their high concentration [9]. Atapattu [6] reports on a peach-shaped yielded region around a moving sphere and a qualitative similarity of the experimental results to those predicted by Beris *et al.* [1]. Recent experimental study differed from Atapattu's conclusions and revealed a break of the fore-and-aft symmetry of the flow even for extremely low Reynolds numbers. The existence of a negative wake behind the sphere [7,8] and an extended flow region in front of it, including a plug-like zone [7], were reported and attributed to the complex rheology of the experimental yield-stress material, which may involve elastic component and thixotropic effects.

Several studies on the measurements of drag on a sphere in viscoplastic fluids [10,11] report on a considerable effect of the surface roughness of the spheres, governing fluid adherence, and an apparent slip at the particle surface affecting the drag force on it. One can assume that surface roughness influences the shape and extent of the yielded region as well as the flow within it. However, no results on this subject such as flow pattern and the influence on the yielded zone shape are available in the literature so far.

The present work is aimed at determining the yielded region shape and flow field around spherical particles with rough and smooth surface, settling in an otherwise quiescent yield-stress medium, making use of precise flow visualization techniques. We have employed particle tracking velocimetry (PTV) and

PIV techniques in an effort to establish the boundary of the yielded region around a spherical particle and record the flow field and its intensity within that region. The paper is organized as follows: Sec. II includes a brief description of the experimental materials, the methods, and the procedure. In Sec. III we present experimental results, including the determination of the yielded regions and the flow fields around various solid spheres in an extended medium. The results are discussed in Sec. IV.

II. EXPERIMENTAL MATERIALS, METHOD, AND PROCEDURE

A. Materials

A gel of Carbopol 940 in aqueous solution was used as a yield-stress material. The solution was prepared by the standard procedure described in the literature, see, e.g., Refs. [7,12]. We have chosen a low concentration, 0.07% w/w, gel in order to minimize elastic and thixotropic effects, while preserving measurable viscoplastic properties [7,13]. The density of the gel at 24 °C is 997 kg/m^3. The material includes 11.4-μm spherical hollow glass tracer particles with density of 1000 kg/m^3, which do not settle under gravity. The gel is prepared at room temperature, at about 23–26 °C, and we used only glass vessels during the preparation of the material and for the gel storage.

The values of rheological properties of Carbopol aqueous gels of similar concentrations reported in the literature (see, e.g., Piau [13]), in particular the yield stress, vary considerably. These variations that can differ by an order of magnitude are caused by properties of the raw materials such as water quality or molecular structure of the Carbopol powder, supplied by various sources, and by the measurement methods. We, therefore, present results of our own study of the prepared Carbopol gel rheology that was performed with the use of a cone and plate ARES RMS-800 Rheometer of Rheometric Scientific in two steps: first, the yield stress of the material is measured making use of the visualization method of Refs. [14,15], and then the other parameters of the chosen rheological model are determined by fitting the experimental data. The details of the procedure can be found in Ref. [15]. In this study we adopt the Herschel-Bulkley constitutive equation, e.g., Ref. [16], that for simple shear flow in the rheometer, reads:

$$\begin{aligned} \tau &= \tau_Y + K\dot{\gamma}^n, \qquad |\tau| \geqslant \tau_Y \\ \dot{\gamma} &= 0, \qquad\qquad\quad |\tau| < \tau_Y \end{aligned} . \tag{1}$$

Here, $\dot{\gamma}$ and τ are unidirectional shear rate and shear stress, respectively, τ_Y is the yield stress, and n and K are Herschel-Bulkley model parameters. At $n = 1$, Eq. (1) becomes the Bingham constitutive equation with plastic viscosity K.

For the 0.07% w/w Carbopol 940 gel at 24 °C the Herschel-Bulkley model parameter, with independently determined yield stress $\tau_Y = 9.07$ Pa, are found to be equal to $n = 0.534$ and $K = 1.322$ Pa·s^n. The parameters predict perfectly the behavior of the gel in the shear rate range of 3 s^{-1} to 1000 s^{-1}, as depicted in Fig. 1. Repeated measurements deviate from this plot by a fraction of a Pascal at most.

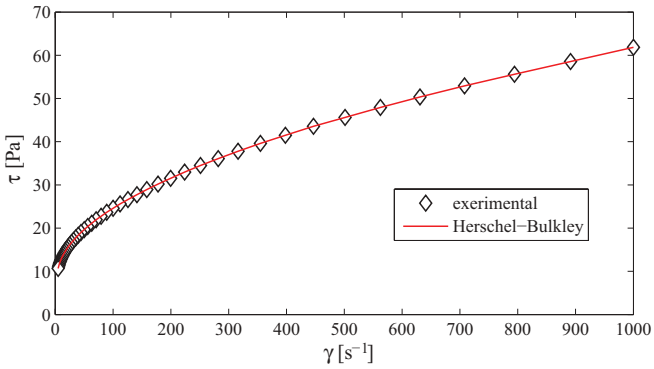

FIG. 1. (Color online) Herschel-Bulkley model fitted to the rheological measurements of Carbopol 0.07% w/w gel at 24 °C.

The rheologic dynamic tests described in Ref. [15] revealed no thixotropic loop and that, at low frequency, the shear storage modulus is low relative to the shear loss modulus. Thus, one can expect only minor elastic and memory effects for the gel. It should be noted, though, that in spite of its absence in the rheometric results, such effects may be evident in the more complex flow around the moving sphere.

Plastic hollow spherical beads of 4.78-mm radius were used for the study of the motion of the spheres inside the yield-stress material. The beads' hollows were filled with polyepoxide glue and provided with small cuts of a steel wire. The wire enabled us to use an electromagnet for the release of the beads into the Carbopol gel without a physical invasive procedure. In addition, the usage of wires of various sizes facilitated control of the bead weight and adjustment of the beads' velocities to the desired levels. The motion of black-colored and noncolored particles was studied. The particles, which were colored with black oil paint (UNIRAC by Nirlat Paint Company), were smoother than the uncolored ones. Roughness of the uncolored spheres was visible, and thus, most likely, the average roughness profile of the spheres was of the order of 50 μm or more, though no accurate measurements were performed. In contrast to this, the colored spheres were visually very smooth.

We report below on the shape of yielded region and velocity field around four types of spherical beads: heavy (0.63 g) and light (0.51 g), colored and uncolored.

B. Apparatus and procedure

The experimental setup for the visualization of the motion of the particles was developed in order to provide a detailed study of the motion in the yield-stress material, using PIV and PTV methods. The scheme of the centerline cut of the experimental apparatus is presented in Fig. 2.

The setup consists of a rectangular glass aquarium (1) of 25 × 25-cm base section and 30-cm height, filled with 0.07% Carbopol aqueous gel. The aquarium is covered with a heavy lid (2). The lid is provided with a hole, engineered for the introduction of solid spheres (3) into the gel-tracer suspension. A steel wire (4) is provided with a stopper and with an electromagnet (5), and was inserted into the lid (2). A bead connected to the wire edge by the electromagnetic force was gently immersed into the gel. When the power supply

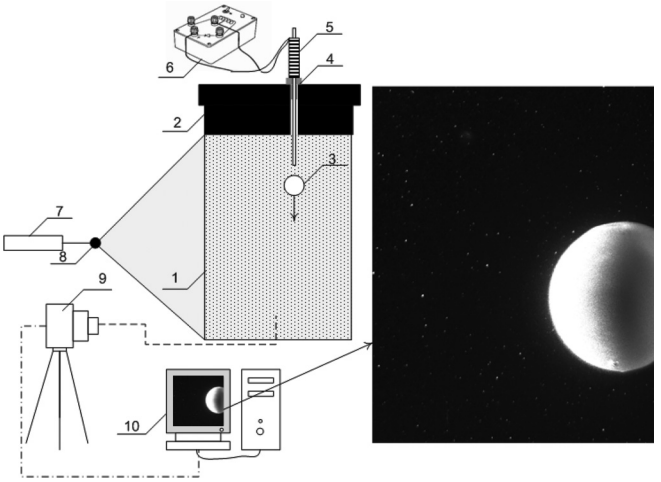

FIG. 2. A schematic description of the experimental apparatus: (1) glass reservoir; (2) plastic lid; (3) solid sphere; (4) nonflexible straight steel wire equipped with a stopper, inserted to a hole in the lid; (5), (6) Electromagnet; (7) Nd:YAG laser; (8) beam splitter; (9) digital PIV photo camera; (10) computer. The enlargement shows a typical photo image of the settling sphere.

was turned off, the bead disconnects from the wire and begins falling under the action of gravity.

As the particle falls through the suspension, a laser device (7,8) is directed through the clear glass walls, illuminating a vertical sheet of the system. The device consists of a high power (160 mJ per pulse) double-pulsed laser Nd:YAG (Twins, Quantel France) (7) and an optical arrangement to convert the laser light to a thin vertical light sheet (8) of 0.1-mm thickness. The light sheet is directed exactly at the center plane of the sphere. Kodak Megaplus ES 1.0 CCD photo camera (9) is used to image the system at various stages of the motion. An external synchronizer, controlled by a computer (10), is used to trigger the camera and the laser. After the run, the inclusion is removed from the experimental fluid and the Carbopol gel is thoroughly remixed in order to recover the homogeneous initial properties of the suspension (see, e.g., Ref. [17]) and enable sequential experiments. It should be noted that a continuous operation of the laser light sheet through the Carbopol solution tank, of several hours, did not result in a detectable change of the gel temperature.

Due to extensive computer resources required for PIV computations, a series of preliminary evaluations were performed before each experiment. These evaluations include a gel homogeneity test, a particle sedimentation test, and a reproducible rheology test. The gel is considered homogeneous if particles reach a terminal velocity after a short distance and continue to move at that speed until the end of the process. Additionally, the particles must travel in a vertical straight line. Keeping these conditions assures that the results of the experiment are valid and the error due to system irregularities is minimized.

C. Data acquisition and processing.

The processing of the experimental results is organized as follows. First, PTV was employed to identify the yielded region boundary. Consequently, the velocity at the yielded region boundary and outside it was ignored and PIV was used to determine the smooth flow field structure inside the yielded region.

The PTV results are processed using the Matlab Particle Tracking Code Repository [18]. The algorithm is based on the assumption that the shift of the tracer in sequential frames is much smaller than the distance between two tracer particles. As a result, a shift of a tracer particle from a frame to the next one is defined.

As PTV processing was aimed at the evaluation of the flowing region boundary, we have been interested in the tracer behavior far from the inclusion. In these regions, the tracers were tracked along image sequence of sufficient length to enable separation between traveling and stationary particles. The separation is confused due to apparent false motion of stationary tracers, which results mostly from fluctuating illumination intensity of the laser system. When the system is better illuminated, the tracer particles reflect more light and seem bigger than when the system is poorly illuminated. The position of the tracer at each image is determined as a center of the best-fitted circle. Thus, when the image of the size of the tracer changes, its position is apparently affected. Hence, stationary particles exhibit an apparent random displacement with zero average shifts, which are induced by the fluctuating illumination intensity of the laser system. It was found that directed motion can be distinguished from the apparent motion of the stationary tracers if the particles are tracked through a long enough image sequence. On the other hand, the dynamic propagation of the yielded region prevents the use of too long sequences. We have found that for each type of inclusion there is some optimal sequence length, which permits tracking of slow directed motion of the tracers near the boundary, while still detecting the stationary ones. The optimal sequences are 34, 30, 24, and 14 images for light rough, light smooth, heavy rough, and heavy smooth beads, respectively.

The position of the tracers at the maximal distance from the inclusion in all directions, which are still moving, is defined as the flowing region boundary (the positions of the drop and the tracers are taken from the last image in the sequence). The accuracy of this method depends mostly on the tracer concentration. The average distance between tracers, which is equal to 0.25 mm, will also be the distance between the last moving and the first stationary particles and hence defines the accuracy of the determination of the yielded region boundary.

Once the yielded region boundary is determined, all the data in the images of the motion detected outside it is ignored and the velocity at the boundary is set to zero. The PIV images of the flow field within the yielded region are analyzed using the MatPIV Matlab toolbox. This package allows tracking the average shift of tracer particles using a cross-correlation method [19]. Note that none of the standard PIV procedures for filtering of the results were used during the analysis. Since the flow field within the yielded region is characterized by a strong variation of the velocity intensity, the techniques that were developed for smoothing the results received from other experiments, e.g., on Newtonian flows, were not needed for the determination of the smooth flow field inside the yield-stress material. Averaging over at least five runs and at least 40 image pairs per system was found sufficient for the determination of the velocity field. This averaging procedure ensured obtaining coherent and meaningful flow results.

TABLE I. Velocities, Reynolds, and Bingham numbers for various beads, calculated based on Herschel-Bulkley model.

Bead type	Sedimentation velocity, mm/s	Re	Bn
Rough light	0.10	$5.95\cdot10^{-5}$	54.1
Smooth light	0.24	$2.15\cdot10^{-4}$	33.9
Rough heavy	0.37	$4.05\cdot10^{-4}$	26.9
Smooth heavy	0.74	$1.12\cdot10^{-3}$	18.6

III. EXPERIMENTAL RESULTS AND DISCUSSION

In this section we present shapes of yielded regions around moving spherical beads of four types—heavy and light, colored (smooth) and uncolored (rough)—determined by PTV and the flow fields in these regions obtained via PIV. The radius of all the spheres is $R = 4.78$ mm. The weights of heavy and light beads are 0.63 and 0.51 g, respectively. The beads fall at constant velocity U, determined from steady change of position with time in sequential exposures.

Define the Reynolds number, $\mathrm{Re} = \rho U R/\eta^*$, with ρ being the gel density, and with the characteristic viscosity of the gel $\eta^* = K(U/R)^{n-1}$ obtained by the Herschel-Bulkley model ($n = 0.543$, $K = 1.322$ Pa·s^n) and the Bingham number, $\mathrm{Bn} = \tau_Y R/(U\eta^*)$, indicating the relative importance of yield stress over viscous forces. The sedimentation velocities and the governing parameters calculated within these definitions are given in Table I.

One can see that in all the cases under consideration the Reynolds numbers are small, $\mathrm{Re} \leqslant O(10^{-3})$, suggesting a creeping flow regime. The Bingham number is relatively high and of the same order of magnitude.

Figure 3 presents the yielded region boundary for light rough [Fig. 3(a)], heavy rough [Fig. 3(b)], light smooth [Fig. 3(c)] and heavy smooth [Fig. 3(d)] single bead systems. The experimental points indicate the position of the farthest moving tracers at the maximal distance from the bead. Different markers indicate three different experimental series. The boundary data and the particle positions and shape are taken from the last frame of the sequence. The sequence lengths are given in Sec. II.

Note that the yielded region around light rough, extremely slow moving beads [Fig. 3(a)] has an almost fore-and-aft symmetrical peach-like shape and resembles the results of numerical simulations available in the literature (see, e.g., Refs. [1,6]). This similarity will be discussed below in more detail. In contrast to this, the yielded regions around faster moving beads [Figs. 3(b)–3(d)] are in closer proximity to the particle surface and exhibit no fore-and-aft symmetry. The bulb shape of the yielded region around the fastest sphere presented in Fig. 3(d) is qualitatively similar to the yielded regions around drops reported in Ref. [15]. Figures 3(b) and 3(c) present intermediate cases.

Figures 4 and 5 present the flow field induced by the rough and smooth, light and heavy beads in the yielded regions defined using PIV. The presentation is separated into maps showing intensity and direction, respectively. The contour maps (right column) refer to the flow intensity depicted by the velocity absolute value, normalized with the drop speed. Unit vectors (left column) present the structure of the velocity field defined using PIV. The given data are averaged over three experimental runs, with at least 70 image pairs in each run.

One can see that, in all the cases, the flow field within the yielded region is characterized by a strong variation of its intensity. The relatively strong flow in the vicinity of the particle surface decays rapidly as the outer boundary is approached.

The flow field around the light rough bead [Fig. 4(a)] is directed downward and is similar to that induced by a sphere moving in the Newtonian fluid. However, a weak negative wake is evident above the particle.

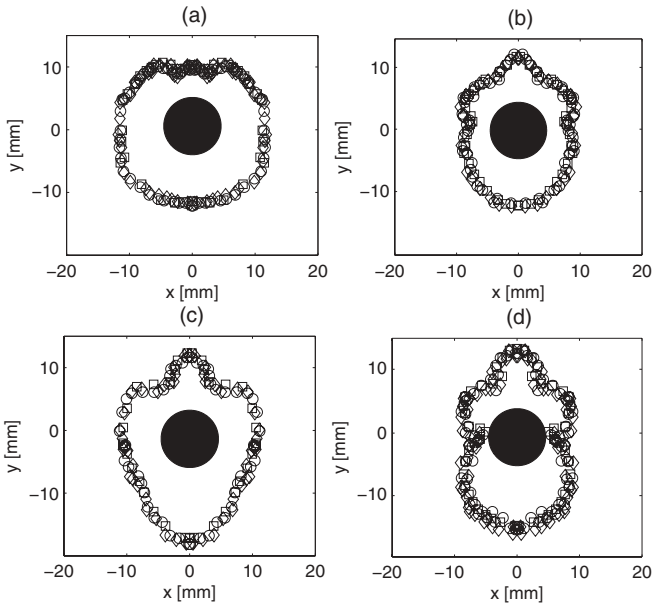

FIG. 3. Yielded region boundaries for: (a) light rough bead; (b) heavy rough bead; (c) light smooth bead; (d) heavy smooth bead. Various markers correspond to separate runs.

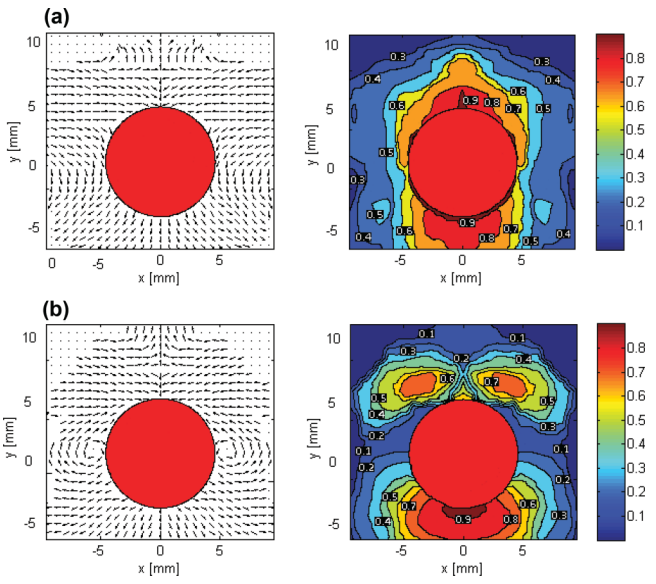

FIG. 4. (Color online) Flow within the yielded region around rough beads settling in an unbounded domain: (a) light bead, (b) heavy bead. Arrows are normalized by the absolute value of the local velocity. Flow intensity is normalized by the bead speed.

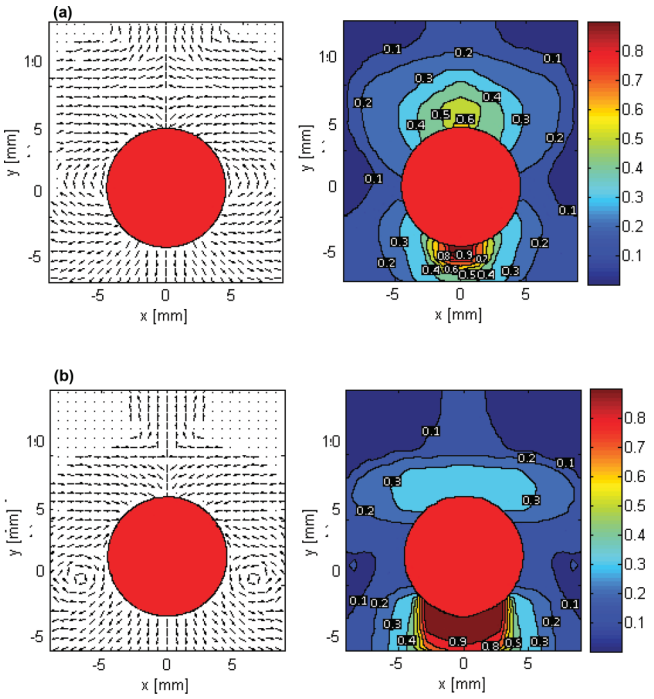

FIG. 5. (Color online) Flow within the yielded region around smooth beads settling in an unbounded domain: (a) light bead, (b) heavy bead. Arrows are normalized to unity by the absolute value of the local velocity. Flow intensity is normalized by the bead speed.

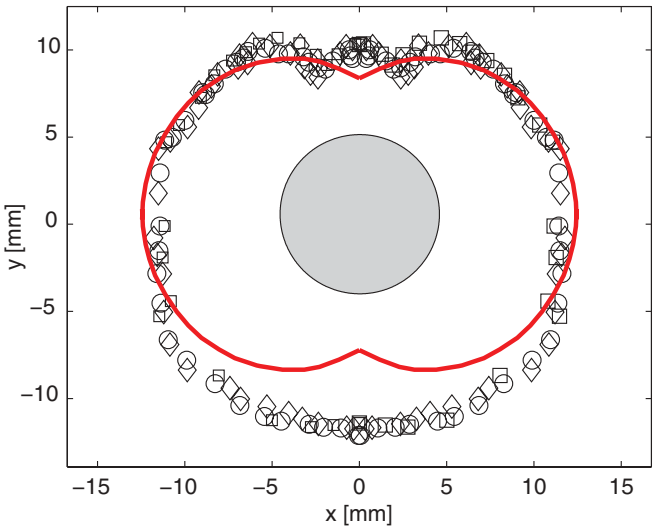

FIG. 6. (Color online) The yielded region around light rough bead (Bn = 54.1, Re = 5.95 10^{-5}), determined using PTV. Various markers correspond to various experimental runs. Solid line is the boundary of the yielded region obtained numerically by Liu *et al.* [2] for a Bingham fluid at Bn = 59.6, Re → 0.

The flow field in the yielded regions around heavy beads and light smooth beads (Figs. 4(b) and 5) is considerably different. A negative wake behind the inclusion is more pronounced and an upward flow is observed in the vicinity of the particle above the equator. Vortices below the particle equator and intensive flow in front of the inclusion are evident as well. This resembles flow fields around solid particles, reported previously (Refs. [7,8]), and the one around drops (see Ref. [15]). This striking similarity can be attributed to a slip at smooth surfaces exhibited by yield-stress fluids.

The apparent slip of Carbopol water gel over smooth surface may be caused by a very thin layer of the low viscosity solvent (water) of the Carbopol solution, which is due to seepage of water from the adjacent gel. In Ref. [15] we used two methods to estimate the thickness of the lubricating (water) layer, d, at the glass surface. The first method was based on the velocity at a stationary boundary measured by PIV, for which the maximal value was $V_w \approx 0.5$ mm/s. As the layer of water, flowing near this wall, is expected to be extremely thin, simple shear flow in this layer can be assumed. If the stress in the boundary between the lubricating layer and the bulk is estimated to be the yield stress, the lubricating layer thickness is approximately equal to: $d = V_w \mu_w / \tau_Y \approx 50$ nm. The second method was based on the rheometric measurements with a titanium cone and a smooth glass plate configuration in comparison to those with titanium cone and plate assuming two-layered simple shear flow and comparing the results. This method provides the lubrication layer thickness estimate of 58 nm at shear rate of 10 s^{-1} (the value anticipated in PIV experiments) and almost linearly growing with the shear rate (see Ref. [15]). This similarity in the result confirms our assumption regarding the wall slip nature.

In Fig. 6 we compare the shape of the yielded region around a slow-moving light rough bead (Bn = 54.1, Re = $5.95 \cdot 10^{-5}$, calculated according to Herschel-Bulkley model), determined using PTV, to the shape of the outer boundary of the yielded region around a bead (Bn = 59.59, Re → 0) calculated numerically by Liu *et al.* [2], making use of the Bingham model (solid line). Markers indicate the yielded region boundary determined using PTV. Different markers correspond to separate experimental runs. $x = 0$ refers to the bead axis. An extremely good matching of the yielded region width is evident. However, numerical simulations result in a considerable underestimation of the length of the yielded region and predict its fore-and-aft symmetry that is not observed experimentally. This discrepancy can be attributed to small elastic effects in the experimental fluid and to the difference in the theoretical and experimental rheological properties.

Note also that the experimental procedure employed in this study is still not refined enough to detect and identify unyielded material, which, according to theoretical predictions, may exist within the yielded region. The detection of such islands requires further development of the reported experimental methods.

IV. CONCLUSIONS

Detailed study of the flow field around spherical solid particles, moving in Carbopol 940 aqueous gel of 0.07% w/w concentration under creeping flow conditions, has been performed using various flow visualization techniques. The motion of isolated inclusions was steady and the yielded region boundary could be determined using PTV, while the structure of the flow field within this boundary was described using

PIV. The combined method, PTV and PIV, yielded excellent description of the yielded region and the flow within it.

For extremely slow moving rough spheres, the form of the outer boundary of the yielded zone is in good agreement with the results of numerical simulations available in the literature. However, the unyielded islands adjacent to the particle reported in these numerical studies were not observed in our experiment. Numerical studies, in their turn, do not predict negative wakes above the spheres, evident in the experiments. The latter appear probably due to the elasticity of the experimental fluid and the recovery process of the microstructure of the Carbopol gel that was ignored in the numerical studies performed so far.

The form of the yielded region and the velocity field around smooth and faster moving spheres are qualitatively different and resemble those around Newtonian drops falling in viscoplastic medium. The similarity of the flow field and yielded region shape around the smooth spheres and drops can be attributed to a slip at the smooth surface. The slip on the bead surface results in a nonzero relative tangential velocity at the sphere surface and, thus, simulates boundary conditions, similar to that at the drops' interface. As a result, the flow fields between the drops and the solid particles become similar. In contrast to this, the apparent slip of the gel over rough surface is prevented by the roughness and the flow field and yielded region shapes become qualitatively different. Note that the flow field induced by the fast moving rough bead is also similar to the flow field around drops. Most likely, in this case the roughness of the surface becomes insufficient to completely prevent apparent slip effect, which is more evident at higher velocities.

To conclude, note that the observed effect of similarity between the flows induced by a smooth solid sphere and by a drop is in a sense opposite to the well-known effect of the "solidification" of contaminated bubble in water (see, e.g., Levich [20]). Rushton and Davies [21] demonstrated that a thin viscous film encapsulating a drop also results in a similar "solidification." The difference between the film of Rushton and Davies [21] and the lubricating water layer that we suppose to exist at the surface of the sphere moving in Carbopol gel, is that the latter is miscible with water and, thus, no return flow appear within this thin layer.

ACKNOWLEDGMENT

O.M.L. acknowledges the support of the Israel Ministry for Immigrant Absorption.

[1] A. N. Beris, J. A. Tsamopoulos, R. C. Armstrong, and R. A. Brown, J. Fluid Mech. **158**, 219 (1985).
[2] B. T. Liu, S. J. Muller, and M. M. Denn, J. Non-Newtonian Fluid Mech. **102**, 179 (2002).
[3] J. Blackery and E. Mitsoulis, J. Non-Newtonian Fluid Mech. **70**, 59 (1997).
[4] M. Beaulne and E. Mitsoulis, J. Non-Newtonian Fluid Mech. **72**, 55 (1997).
[5] B. D. de Besses, A. Magnin, and P. Jay, AIChE **50**, 262710 (2004).
[6] D. D. Atapattu, B. P. Chhabra, and P. H. T. Uhlherr, J. Non-Newtonian Fluid Mech. **59**, 245 (1995).
[7] A. M. V. Putz, T. I. Burghelea, I. A. Frigaard, and D. M. Martinez, Phys. Fluids **20**, 033102 (2008).
[8] B. Gueslin, L. Talini, B. Herzhaft, Y. Peysson, and C. Allain, Phys. Fluids **18**, 103101 (2006).
[9] M. Raffel, C. E. Willert, and J. Kompenhans, *Particle Image Velocimetry: A Practical Guide*, 2nd ed. (Springer, Berlin, 2007).
[10] L. Jossic and A. Magnin, AIChE J. **47**, 2666 (2001).
[11] O. Merkak, L. Jossic, and A. Magnin, J. Non-Newtonian Fluid Mech. **133**, 99 (2001).
[12] Yu. Holenberg, O. Lavrenteva, and A. Nir, Rheol. Acta **50**, 375 (2010).
[13] J. M. Piau, J. Non-Newtonian Fluid Mech. **144**, 1 (2007).
[14] A. Magnin and J. M. Piau, J. Non-Newtonian Fluid Mech. **36**, 85 (1990).
[15] Yu. Holenberg, O. M. Lavrenteva, A. Liberzon, U. Shavit, and A. Nir, J. Non-Newtonian Fluid Mech. (2012), doi: 10.1016/j.jnnfm.2012.09.013
[16] G. R. Burgos, A. N. Alexandrou, and V. Entov, J. Non-Newtonian Fluid Mech. **43**, 463 (1999).
[17] D. D. Atapattu, B. P. Chhabra, and P. H. T. Uhlherr, J. Non-Newtonian Fluid Mech. **38**, 31 (1990).
[18] D. Blair and E. Dufresne, Matlab Particle Tracking Code Repository (2007), http://physics.georgetown.edu/matlab/.
[19] J. K. Sween, An Introduction to MatPIV v.1.6.1, Eprint No. 2 (2004) ISSN 0809-4403, Department of Mathematics University of Oslo, http://www.math.uio.no/∼jks/matpiv.
[20] V. G. Levich, *Physicochemical Hydrodynamics* (Prentice-Hall, Englewood Cliffs, NJ, 1962).
[21] E. Rushton and G. A. Davies, Int. J. Multiphase Flow **9**, 337 (1983).